THE JOURNAL OF PHYSICAL CHEMISTRY A
A JOURNAL OF THE AMERICAN CHEMICAL SOCIETY

pubs.acs.org/JPCA Article

Computational Analysis of the Superoxide Dismutase Mimicry Exhibited by a Zinc(II) Complex with a Redox-Active Organic Ligand

Evangelos Miliordos,* Jamonica L. Moore, Segun V. Obisesan, Julian Oppelt, Ivana Ivanović-Burmazović, and Christian R. Goldsmith*

Cite This: J. Phys. Chem. A 2024, 128, 1491−1500 Read Online

ACCESS | Metrics & More | Article Recommendations | Supporting Information

ABSTRACT: Previously, we found that a Zn(II) complex with the redox-active ligand *N*-(2,5-dihydroxybenzyl)-*N*,*N*′,*N*′-tris(2-pyridinylmethyl)-1,2-ethanediamine (H_2qp1) was able to act as a functional mimic of superoxide dismutase, despite its lack of a redox-active transition metal. As the complex catalyzes the dismutation of superoxide to form O_2 and H_2O_2, the quinol in the ligand is believed to cycle between three oxidation states: quinol, quinoxyl radical, and *para*-quinone. Although the metal is not the redox partner, it nonetheless is essential to the reactivity since the free ligand by itself is inactive as a catalyst. In the present work, we primarily use calculations to probe the mechanism. The calculations support the inner-sphere decomposition of superoxide, suggest that the quinol/quinoxyl radical couple accounts for most of the catalysis, and elucidate the many roles that proton transfer between the zinc complexes and buffer has in the reactivity. Acid/base reactions involving the nonmetal-coordinating hydroxyl group on the quinol are predicted to be key to lowering the energy of the intermediates. We prepared a Zn(II) complex with *N*-(2-hydroxybenzyl)-*N*,*N*′,*N*′-tris(2-pyridinylmethyl)-1,2-ethanediamine (Hpp1) that lacks this functional group and found that it could not catalyze the dismutation of superoxide; this confirms the importance of the second, distal hydroxyl group of the quinol.

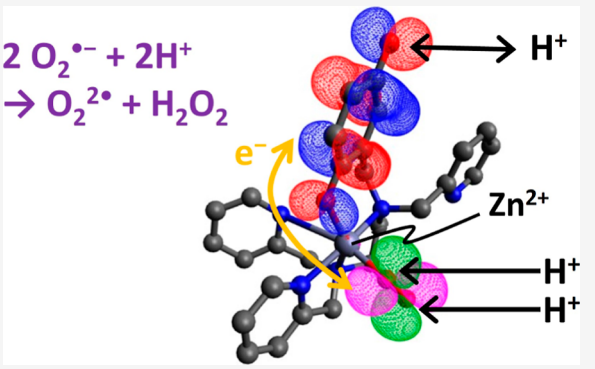

INTRODUCTION

Superoxide dismutases (SODs) are enzymes that catalyze the degradation of superoxide ($O_2^{\bullet-}$) to dioxygen (O_2) and hydrogen peroxide (H_2O_2, eq 1).

$$2O_2^{\bullet-} + 2H^+ \rightarrow O_2 + H_2O_2 \quad (1)$$

All known SODs employ a redox-active transition metal in the active site, containing either manganese, iron, nickel, or copper.[1,2] The metals act as redox partners for $O_2^{\bullet-}$. During catalysis, the metals cycle between two oxidation states, with the more highly oxidized metal ion oxidizing $O_2^{\bullet-}$ to O_2 and the more reduced metal ion reducing $O_2^{\bullet-}$ to peroxide, which gets protonated to H_2O_2.

The overproduction of $O_2^{\bullet-}$ and other reactive oxygen species (ROS) has been correlated to a diverse group of health conditions, including inflammatory, cardiovascular, and neurological disorders.[3−11] This has motivated us and other researchers to develop small-molecule mimics of SOD that could catalytically lower ROS levels in vivo. In turn, this could potentially alleviate the symptoms of these health conditions or even halt the progression of the diseases altogether.

Most functional mimics of SOD resemble the enzymes in that they contain redox-active metal ions.[1,12−34] The most active of these mimetics, as assessed by the k_{cat} rate constants for their in vitro reactions with superoxide, have been manganese complexes with either cationic porphyrinic or pentaazamacrocyclic ligands.[23−32] Certain classes of metal-free compounds, chiefly nitroxides and fullerene derivatives, have also been found to catalyze the degradation of $O_2^{\bullet-}$ but at rates that are much slower than those of both the enzymes and the best transition metal-containing SOD mimics.[23,27,35,36]

Recently, we reported functional SOD mimics that rely on a third strategy: complexing a redox-active organic molecule to a redox-inactive metal ion, specifically Zn(II).[37,38] The first two mimics use *N*-(2,5-dihydroxybenzyl)-*N*,*N*′,*N*′-tris(2-pyridinylmethyl)-1,2-ethanediamine (H_2qp1) and *N*,*N*′-bis(2,5-dihydroxybenzyl)-*N*,*N*′-bis(2-pyridinylmethyl)-1,2-ethanediamine (H_4qp2) as the ligands; the quinols in these molecules can be oxidized by two electrons to *para*-quinones.[39] Both [Zn(H_2qp1)(OTf)](OTf) (**1**) and [Zn(H_4qp2)](OTf)$_2$ (**2**) catalyze the dismutation of $O_2^{\bullet-}$ at rates that were both much faster than those of purely organic antioxidants and comparable to those of manganese-containing SOD

Received: November 8, 2023
Revised: January 26, 2024
Accepted: January 29, 2024
Published: February 14, 2024

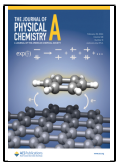

Scheme 1. Structures of [Zn(Hqp1)]$^+$, Its Conjugate Base [Zn(qp1)], Its Deprotonated and One-Electron Oxidized Form [Zn(qp1)]$^{\bullet+}$, and the Deprotonated/Two-Electron Oxidized Product [Zn(qp1)]$^{2+}$. The *para*-Quinone in [Zn(qp1)]$^{2+}$ May Bind Weakly to the Metal Center

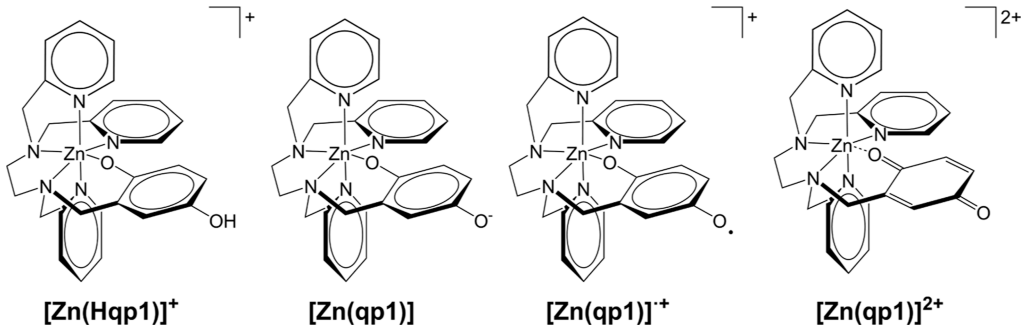

mimics.[37,38] Both complexes differ from all other small-molecule SOD mimics in that their activities are enhanced rather than inhibited in phosphate buffer. At physiological pH (pH ∼ 7.4), **1** deprotonates to [Zn(Hqp1)]$^+$ (Scheme 1);[37] **2** similarly deprotonates to the monocationic [Zn(H$_3$qp2)]$^+$.[38]

The diamagnetism of Zn(II) limits our ability to spectroscopically monitor the stoichiometric and catalytic reactions between the zinc complexes and $O_2^{\bullet-}$. The observed UV/vis bands come exclusively from intraligand transitions and provide evidence for the oxidation of the quinol portion of H$_2$qp1 to a *para*-quinone (qp1); the oxidation of the Zn(II) compound to a mixture of the starting complex and the two-electron oxidized form [Zn(qp1)]$^{2+}$ is also supported by mass spectrometry.[37] Although it was not observed in the catalysis for the initial report, the chemistry was believed to proceed through the Zn(II) complex with the one-electron-oxidized ligand Hqp1$^{\bullet}$, which can deprotonate to qp1$^{\bullet-}$. With **2**, low-temperature UV/vis analysis suggested that semiquinone radicals were indeed produced.[38] Low-temperature mass spectrometry data for **1** are consistent with the formation of a Zn(II)−OOH species and an inner-sphere mechanism of superoxide dismutation,[37] but a similar species was not detectable for **2**.[38] Furthermore, the MS data for **1** could instead correspond to a Zn(II)−OH species with an oxygenated ligand. Regrettably, these complexes lack charge transfer bands that would enable us to confirm the bound OOH groups through resonance Raman spectroscopy.

Here, we test the viability of the proposed mechanism for superoxide degradation using density functional theory (DFT). We assess the structures and energies of various proposed intermediates derived from **1**; we selected this over **2** to avoid complications from the inclusion of a second redox-active quinol. Our chief interests are (1) probing the feasibilities of inner-sphere reduction and oxidation of $O_2^{\bullet-}$ with a redox-inactive metal, (2) determining whether the qp1$^{\bullet-}$/Hqp1$^-$ or qp1/qp1$^{\bullet-}$ redox couple features more prominently in the catalysis, (3) elucidating the electronic structure of the [Zn(qp1$^{\bullet-}$)]$^+$ species, (4) understanding how acid/base chemistry with the solvent and/or buffer impacts the mechanistic cycle, and (5) predicting how activity could be improved through synthetic modifications to the catalyst. We also prepared a Zn(II) complex with *N*-(2-hydroxybenzyl)-*N*,*N*′,*N*′-tris(2-pyridinylmethyl)-1,2-ethanediamine (Hpp1, Scheme 2); this compound differs from the Zn(II)−H$_2$qp1 complex in that it lacks the distal, noncoordinating hydroxyl group. The Hpp1 complex was not a competent catalyst for superoxide dismutation.

Scheme 2. Structure of H$_4$qp2 and Hpp1 with Metal-Coordinating Atoms Highlighted

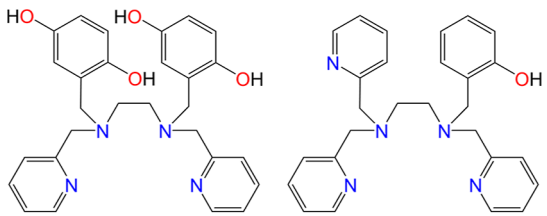

METHODS

Materials. Most chemicals and solvents were purchased from Sigma-Aldrich and used without further purification. Diethyl ether (ether) and methanol (MeOH) were purchased from Fisher. Deuterated methanol (CD$_3$OD) was purchased from Cambridge Isotopes. *N*-(2-Hydroxybenzyl)-*N*,*N*′,*N*′-tris-(2-pyridinylmethyl)-1,2-ethanediamine (Hpp1) was synthesized as previously described.[40]

Instrumentation. All nuclear magnetic resonance (NMR) data were collected on a 500 mHz AV Bruker NMR spectrometer. All NMR resonance peak frequencies were referenced to internal standards. UV/vis data were collected on a Varian Cary 50 spectrophotometer and analyzed using software from WinUV Analysis Suite. High-resolution mass spectrometry data were obtained at the Mass Spectrometer Center at Auburn University on a Bruker Microflex LT MALDI-TOF mass spectrometer via direct probe analysis operated in positive ion mode. Infrared (IR) data were obtained with a Shimadzu IR Prestige-21 Fourier transform infrared spectrophotometer. Elemental analysis (C, H, and N) was performed by Atlantic Microlab (Norcross, GA); the sample was dried under vacuum and placed under a N$_2$ atmosphere prior to shipment.

Kinetic Assessment of SOD Activity. The ability of the Hpp1 complex to catalytically degrade superoxide was tested by a direct method using stopped-flow techniques described in a previous publication from one of our laboratories.[41] Experiments were carried out using syringes 1, 2, and 3 on a Biologic SFM-400 instrument that was equipped with an Energetiq LDLS ENQ EQ-99-FC laser-driven light source and a J&M TIDAS diode array detector (integration time = 0.5 ms, λ = 180−724 nm). The source of superoxide was commercially available KO$_2$ dissolved in dry and nonbuffered dimethyl sulfoxide (DMSO) with [$O_2^{\bullet-}$] ≈ 1−2 mM. The Zn(II)−

https://doi.org/10.1021/acs.jpca.3c07403
J. Phys. Chem. A 2024, 128, 1491−1500

Scheme 3. Illustration of the mer and fac Conformations of $[Zn(Hqp1)]^+$. For the mer Conformer, Superoxide Necessarily Coordinates *cis* to the Quinolate upon Displacement of a Pyridine. For the fac Conformer, Superoxide Can Coordinate Either *trans* (fac/trans) Or *cis* (fac/cis) to the Quinolate upon Displacement of a Pyridine Ring. The Red Arrows Show the Possible Trajectories of $O_2^{\bullet-}$, with the Potentially Displaced Pyridines Being Highlighted in Blue

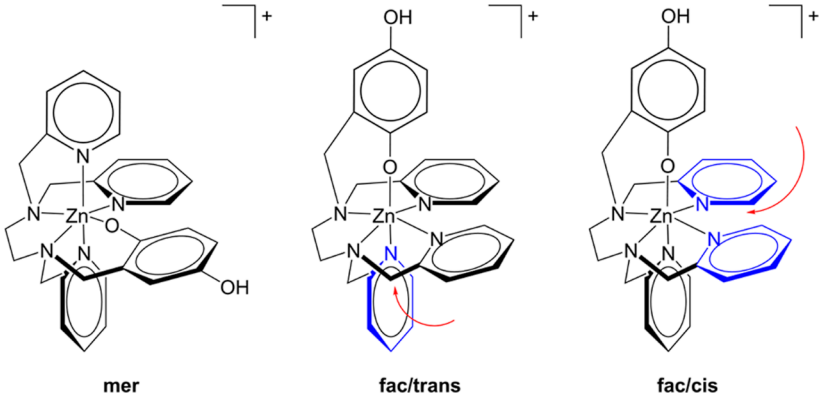

Hpp1 complex was tested at four different concentrations between 0.9 and 9 μM in aqueous solutions buffered with 3-(*N*-morpholino)propanesulfonic acid (MOPS) to pH 7.4. The ionic strength of all solutions was 150 mM. The aqueous solution containing the Zn(II) complex was mixed in a 9:1 ratio with the superoxide solution in DMSO using a high-density mixer. The initial concentration of the superoxide is determined from the intensity of the UV band at 250 nm as assessed immediately after stopped-flow mixing of the superoxide DMSO solution with the appropriate buffer. The 250 nm band is characteristic for superoxide and has well-known and -established molar extinction coefficients for each buffer and pH used.[42] In each experiment, the concentration of superoxide exceeded that of the metal-containing catalyst by at least 10-fold to ensure catalytic conditions. Millipore water was used for the preparation of the buffer solutions. All prepared buffers were treated with Chelex 100 sodium exchange resin for at least 12 h before use in order to remove adventitious metal ions. Data analysis was performed using BioKine V4.66 software.

Computational Details. The structures of possible intermediates were optimized by DFT. To obtain the calculated structures, we used the MN15 functional[43] combined with the 6-31g(d,p) basis set for all atoms except oxygen, which instead uses 6-31g+(d,p), which has an additional series of diffuse functions.[44−48] The addition of diffuse functions on oxygen was essential to reasonably predict the electron affinity of O_2 (0.55 eV vs the experimental value of 0.45 eV).[49] The chosen functional previously performed well for systems containing transition metals and systems bearing noncovalent interactions.[50,51] We applied the solvent model based on density (SMD) methodology to account for solvent (water) effects.[52] All structures were found to have only real vibrational harmonic frequencies. Free-energy corrections at 20 °C and 1.0 atm were calculated via the harmonic approximation, and all calculations were carried out with Gaussian16.[53]

Synthesis. *[N-(2-Hydroxybenzyl)-N,N′,N′-tris(2-pyridinylmethyl)-1,2-ethanediamine]zinc(II) Triflate {[Zn(Hpp1)](OTf)$_2$, **3**}.* Hpp1 (0.100 g, 0.228 mmol) and $Zn(OTf)_2$ (0.083 g, 0.228 mmol) were dissolved in 2 mL of MeOH under N_2 and stirred at room temperature. After 16 h, 2 mL of ether was added to the solution to precipitate the crude product. The solid was further purified by washing with MeOH/ether (1:5 v/v) and dried under N_2 to give the product as a white powder (0.100 g, 55% yield). ^{1}H NMR (500 MHz, CD_3OD, 293 K): δ 8.64 (d, J = 5.4 Hz, 2H), 8.34 (m, 1H), 8.17−8.21 (d, J = 6.4 Hz, 2H), 7.70−7.81 (d, J = 13.6 Hz, m, 7H), 6.90 (m, 2H), 6.78 (m, 2H), 4.66−4.73 (d, J = 16.4 Hz, 3H), 4.49 (m, 1H), 4.28−4.36 (m, 1H), 4.25 (m, 1H), 3.51 (m, 2H), 3.50 (m, 1H), 3.32 (m, 1H), 2.87 (d, J = 10.9 Hz, 2H), 2.23 (d, J = 11.1 Hz, 1H). ^{13}C NMR (125 MHz, CD_3OD, 293 K): δ 157, 155, 148, 147, 146, 141, 132, 125, 124, 121, 120, 119, 115, 65, 60, 55, 54, 52, 48, 47, 15. Optical spectroscopy (MeOH, 293 K): 239 nm (ε = 2000 M^{-1} cm^{-1}), 273 nm (ε = 1800 M^{-1} cm^{-1}). IR (cm^{-1}): 3331 (m), 1609 (s), 1574 (w), 1516 (m). 1487 (w), 1444 (s), 1275 (w), 1236 (w), 1221 (s), 1155 (s), 1107 (w), 1080 (m), 1056 (m), 1025 (s), 979 (w), 945 (w), 828 (m), 760 (s), 724 (w), 633 (s), 597 (w), 572 (m), 514 (s). MS (ESI): calcd for $[Zn^{II}(Hpp1)]^{2+}$, 251.5832; found, 251.5826, calcd for $[Zn^{II}(Hpp1)(HCOO^-)]^+$, 548.1612; found, 548.1642, calcd for $[Zn^{II}(Hpp1)(OTf)]^+$, 652.1124; found, 652.1170. Elemental analysis: calcd for $C_{29}H_{29}N_5ZnF_6O_7S_2{\cdot}2H_2O$: C, 41.29%; H, 3.94%; N, 8.30%; found, C, 40.98%; H, 3.92%; N, 8.12%.

RESULTS AND DISCUSSION

The Zn(II)−H_2qp1 complex (**1**) can potentially be oxidized by up to two electrons and is either singly or doubly deprotonated. At physiological pH, **1** spontaneously deprotonates to $[Zn(Hqp1)]^+$;[37] consequently, the metal-bound O atom from the quinol-derived portion of the ligand remains deprotonated in all investigated intermediates. The possible general reaction steps considered in this study for the degradation of superoxide to hydrogen peroxide (eq 1) facilitated by $[Zn(Hqp1)]^+$ in phosphate buffer are listed below

$$[Zn(Hqp1)]^+ + O_2^{\bullet-} \rightarrow [O_2Zn(Hqp1)]^{\bullet} \quad (A)$$

$$[O_2Zn(Hqp1)]^{\bullet} + H_2PO_4^- \rightarrow [HOOZn(Hqp1)]^{\bullet+} + HPO_4^{2-} \quad (B)$$

$$[HOOZn(Hqp1)]^{\bullet+} + H_2PO_4^- \rightarrow [H_2O_2Zn(Hqp1)]^{\bullet,2+} + HPO_4^{2-} \quad (C)$$

$$[H_2O_2Zn(Hqp1)]^{\bullet,2+} \rightarrow [Zn(Hqp1)]^{\bullet,2+} + H_2O_2 \quad (D)$$

https://doi.org/10.1021/acs.jpca.3c07403
J. Phys. Chem. A 2024, 128, 1491−1500

Table 1. Relative Free Energies (kcal/mol) for the Products of Reaction Steps A–F for the Various Conformations of the Zn(II) Complex with Respect to the Lowest-Energy IS

species	$[Zn(Hqp1)]^{+}$[a]	$[Zn(qp1)]$[a,b]	$[Zn(qp1)]$[b,c]	$[Zn(qp1)]$[b,d]	$[Zn(qp1)]^{\bullet+}$[a,e]
(IS)[f] $[Zn(Hqp1)]^{+}/[Zn(qp1)]/[Zn(qp1)]^{\bullet+}$, $2H_2PO_4^{-}$, $2O_2^{\bullet-}$	0.0	15.5	18.4	18.4	99.3
(A) $[O_2Zn(Hqp1)]^{\bullet}/[O_2Zn(qp1)]^{\bullet-}/[O_2Zn(qp1)]^{2\bullet}(S = 0)$, $2H_2PO_4^{-}$, $O_2^{\bullet-}$	12.7	26.6	26.8	27.8	113.2
(B) $[HOOZn(Hqp1)]^{\bullet+}/[HOOZn(qp1)]^{\bullet}/[HOOZn(qp1)]^{+}$, $H_2PO_4^{-}$, HPO_4^{2-}, $O_2^{\bullet-}$	21.4	12.3	5.9	8.0	110.0
(C) $[H_2O_2Zn(Hqp1)]^{\bullet2+}/[H_2O_2Zn(qp1)]^{\bullet+}/[H_2O_2Zn(qp1)]^{2+}$, $2HPO_4^{2-}$, $O_2^{\bullet-}$	12.6	2.6	4.4	5.9	110.1
(D) $[Zn(Hqp1)]^{\bullet2+}/[Zn(qp1)]^{\bullet+}/[Zn(qp1)]^{2+}$ $2HPO_4^{2-}$, $O_2^{\bullet-}$, H_2O_2	6.0	−3.1	−1.7	−1.7	102.0
(E) $[O_2Zn(Hqp1)]^{2\bullet,+}(S = 1)$[g]$/[O_2Zn(qp1)]^{2\bullet}(S = 1)$[h]$/[O_2Zn(qp1)]^{\bullet+}$[i], $2HPO_4^{2-}$, H_2O_2	−0.2	10.8	8.8	6.7	100.2
(F) $[Zn(Hqp1)]^{+}/[Zn(qp1)]/[Zn(qp1)]^{\bullet+}$, $2HPO_4^{2-}$, $O_2^{2\bullet}(S = 1; X^3\Sigma_g^{-})$, H_2O_2	−9.5	6.1	8.9	8.9	89.9

[a]Structure corresponds to the **mer** conformation in Scheme 3. [b]The free-energy difference between $[Zn(Hqp1)]^{+}$ and $[Zn(qp1)]$ is fixed at +15.5 kcal/mol to account for the acid/base free-energy difference in the solution; see text. [c]Structure corresponds to the **fac**/**cis** conformation and trajectory of superoxide binding in Scheme 3. [d]Structure corresponds to the **fac**/**trans** conformation and trajectory of superoxide binding in Scheme 3. [e]The $[Zn(qp1)]^{\bullet+}$ free energy is obtained as the $[Zn(qp1)]$ free energy plus the $[Zn(qp1)]^{\bullet+}/[Zn(qp1)]$ free energy difference. [f]Initial species. [g]$O_2^{2\bullet}(S = 1)$,$[Zn(Hqp1)]^{+}$ complex. [h]$S = 0$ is just 0.03 kcal/mol higher. [i]$O_2^{2\bullet}(S = 1)$,$[Zn(qp1)]^{\bullet+}$ complex.

$$[Zn(Hqp1)]^{\bullet,2+} + O_2^{\bullet-} \rightarrow [O_2Zn(Hqp1)]^{2\bullet,+} \quad (E)$$

$$[O_2Zn(Hqp1)]^{2\bullet,+} \rightarrow [Zn(Hqp1)]^{+} + O_2^{2\bullet} \quad (F)$$

In step A, one pyridine group of the H_2qp1 ligand detaches from Zn(II) allowing $O_2^{\bullet-}$ to coordinate to the metal center. Our calculations show that the pentacoordinate complex with a detached pyridine is only ∼7 kcal/mol higher in energy than the hexacoordinate complex, suggesting that the two species may exchange and that a dissociative mechanism for ligand exchange is plausible. In reaction B, a proton is transferred from a dihydrogen phosphate from the buffer to the terminal oxygen atom of the coordinated superoxide while an electron is transferred from $Hqp1^{-}$ to the superoxide. This reduces and protonates superoxide ($O_2^{\bullet-}$) to hydroperoxide (OOH^{-}). In reaction C, a second proton is provided by another equiv of dihydrogen phosphate to form H_2O_2, which is subsequently released in step D. In step E, a second $O_2^{\bullet-}$ binds to Zn(II). The superoxide reduces the quinol-derived portion of the ligand as it oxidizes to O_2 in step (F). Analogous routes are studied for reactions starting from $[Zn(qp1)]$ and $[Zn(qp1)]^{\bullet+}$, which differ from $[Zn(Hqp1)]^{+}$ by the removal of a proton and a net hydrogen atom, respectively. The Supporting Information provides more details on reaction steps A–F starting from these two species.

Reaction Step A—Initial Coordination of Superoxide. The most stable $[Zn(Hqp1)]^{+}$ species adopts two structures that differ with respect to the coordinating position of the quinolate relative to those of the two tertiary amines. The **mer** and **fac** conformers are shown in Scheme 3, with the former being ∼5 kcal/mol more stable. In the **fac** case, $O_2^{\bullet-}$ can potentially bind either next to (**fac**/**cis**) or across from (**fac**/**trans**) the quinolate when it displaces a pyridine ring, as visualized by the red arrows in Scheme 3. In the **mer** conformation, an incoming $O_2^{\bullet-}$ necessarily occupies a position *cis* to the quinolate upon displacing one of the pyridines. Similar structures are possible for $[Zn(qp1)]$ and $[Zn(qp1)]^{\bullet+}$. Our calculations confirm our expectations that placing the two redox-active components, quinolate and $O_2^{\bullet-}$, closer together facilitates the electron transfer between these groups (see below) and that orienting these *cis* to each other will result in more rapid SOD mimicry.

The theoretically predicted low energy differences between the **mer** and **fac** structures are consistent with the previously obtained data. Again, these designations refer to the relative orientations of the quinolate and the two tertiary amines. ^1H NMR data for **1** suggest the existence of multiple species in solution,[37] and it is likely that both the **mer** and **fac** isomers are present and exchanging with each other. In our initial report,[37] however, we were unable to unambiguously identify, differentiate, and quantify these isomers. The hydroxy group in the quinolate could potentially be deprotonated, leading to $[Zn(qp1)]$. The latter is initially 15.5 kcal/mol higher in energy but becomes much more energetically feasible after the reaction with superoxide (see below). The energy difference of 15.5 kcal/mol between $[Zn(Hqp1)]^{+}$ and $[Zn(qp1)]$ is calculated with eq 2

$$\Delta G = 2.3\ R\ T\ pK_a \quad (2)$$

where the pK_a corresponds to $[Zn(Hqp1)]^{+} \rightleftharpoons [Zn(qp1)] + H^{+}$ and has been estimated to be 11.6.[54] We were unable to directly measure this value due to precipitation of the complex above pH 9.0.[37] Computationally, the same energy difference can be estimated by comparing $[Zn(Hqp1)]^{+} + HPO_4^{2-}$ and $[Zn(qp1)]^{+} + H_2PO_4^{-}$; this provides an alternative value of 11.2 kcal/mol. We used the 15.5 kcal/mol value in the rest of our study, but the conclusions and predicted mechanism remained the same for either value.

The relative free energies for reaction step A using $H_2PO_4^{-}$ as a proton donor and $[Zn(Hqp1)]^{+}$, $[Zn(qp1)]$, or $[Zn(qp1)]^{\bullet+}$ as the acceptor are listed in Table 1, and the corresponding free energy diagrams (FEDs) are shown in Figure 1. All free energies are referenced to those of the lowest-energy reacting species: $[Zn(Hqp1)]^{+}$(**mer**) + $2H_2PO_4^{-}$ + $2O_2^{\bullet-}$. The **mer** conformers are our primary focus for all three starting species since they are the most stable, but the **fac** conformers for the redox-active $[Zn(qp1)]$ species are also considered with both the **cis** and **trans** trajectories for the coordinating superoxide. In all six steps (A–F), the mass, charge, and spin (number of unpaired electrons) are conserved. The FEDs for $[Zn(Hqp1)]^{+}$(**mer**) and $[Zn(qp1)]^{\bullet+}$(**mer**) are parallel, with the latter lying higher by +99.3 kcal/mol. Therefore, only the former is included in Figure 1. The high similarity of these species results from the fact that $[Zn(Hqp1)]^{+}$ and $[Zn(qp1)]^{\bullet+}$ only differ by a single $H^{\bullet}$; the formed "observer" O–H bond does not significantly impact the geometries. The enthalpy and entropy changes

https://doi.org/10.1021/acs.jpca.3c07403
J. Phys. Chem. A 2024, 128, 1491−1500

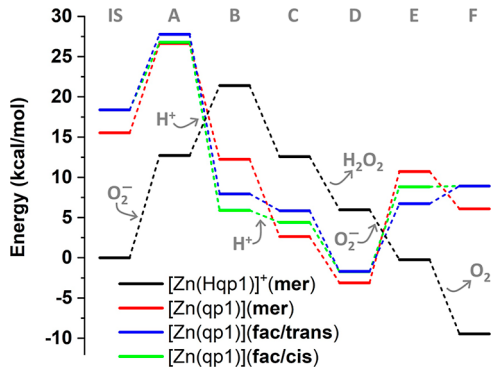

Figure 1. FEDs for the initial species (IS) and the intermediate species formed from steps A−F in Table 1 for superoxide dismutation catalyzed by $[Zn(Hqp1)]^+$ (**mer**) and $[Zn(Hqp1)]$ (**mer**, **fac**/**trans**, and **fac**/**cis**).

during the initial insertion of $O_2^{\bullet-}$ increase the free energy in all cases by as much as 11−14 kcal/mol. $O_2^{\bullet-}$ remains largely ionic with one localized unpaired electron in its π^* orbital (Figure 2).

Reaction Step B—Proton Transfers Facilitate Intramolecular Superoxide Reduction. In step B, the Zn(II)-bound superoxide abstracts a proton from the solution, as it accepts one electron from the quinol-derived portion of the H_2qp1 ligand via a concerted proton-coupled electron transfer (PCET). Our calculations show that the unpaired electron is delocalized throughout the oxidized quinolate (Figure 2). At this point in the reaction, the free energy for the $[Zn(Hqp1)]^+$-derived intermediate is substantially higher than that derived from $[Zn(qp1)]$. The PCET for the **mer** conformer of the $[Zn(qp1)]$-derived intermediate is favorable, with $\Delta G = -14.4$ kcal/mol; ΔG for the analogous PCET reactions starting from the **fac**/**cis** and **fac**/**trans** conformers, conversely, are −20.1 and −19.8 kcal/mol, respectively. As a result, the free energy of intermediate B, where the electron transfer has occurred, is lower for **fac**/**cis** than **fac**/**trans** (Figure 1). The $[HOOZn(qp1)]^{\bullet}$ product is lower in energy than its conjugate acid $[HOOZn(Hqp1)]^{\bullet+}$, and it is at this step that the two FEDs corresponding to the $[Zn(Hqp1)]^+$ and $[Zn(qp1)]$ starting materials cross each other. Initially deprotonating the OH group of the semiquinolate anion enables the subsequent PCET to proceed through lower-energy intermediates, facilitating the formation of OOH.

To understand why the deprotonation of the OH of the semiquinolate anion renders electron transfer more thermodynamically favorable, we calculated the ionization energies of $Hqp1^-$, $qp1^{2-}$, and $qp1^{\bullet-}$—the redox-active moieties of $[Zn(Hqp1)]^+$, $[Zn(qp1)]$, and $[Zn(qp1)]^{\bullet+}$—to see which species most readily relinquishes an electron. The $qp1^{2-}$ is the only one of the three to be stabilized upon ionization, with a negative ionization energy of −3.5 eV. Both $Hqp1^-$ and $qp1^{\bullet-}$, conversely, have positive ionization energies (1.7 and 1.9 eV), indicating that they prefer to accept an electron. The formation of $qp1^{2-}$ in solution from *para*-quinone-containing qp1 would require the provision of two electrons. Alternatively, the dianionic ligand can also be formed from H_2qp1 by removing two protons and stabilizing $qp1^{2-}$ over $qp1^-$. This second path is not feasible for the metal-free ligands since $qp1^-$ is more stable than $qp1^{2-}$ by 3.5 eV. Our calculations indicate that Zn(II) is crucial to forming and electrostatically stabilizing $qp1^{2-}$. One last note is that a change in the conformation at this reaction step is also possible since the $[Zn(Hpq1)]^+$ FED crosses with the FEDs of all three (**mer**, **fac**/**trans**, and **fac**/**cis**) conformations of $[Zn(qp1)]$ (Figure 1). Independently of the conformation adopted, the overall mechanism and process will remain the same since all three FEDs are "parallel" to each other and all cross again with the $[Zn(Hqp1)]^+$ FED at step E.

The importance of this deprotonation is corroborated by the previously obtained kinetic data. When the pH of the solution is raised from 7.4 to 8.1, the k_{cat} rate constant for superoxide dismutation by **1** increases by ∼40%.[37] The improved activity of the Zn(II)−H_2qp1 catalyst under basic conditions is unusual. Many other SOD mimics, including the manganese analog of **1**, often lose activity and become less effective catalysts under more basic conditions.[12−14,16,17,34,41,55−57]

Reaction Steps C and D—Protonation of Hydroperoxide and Release of Hydrogen Peroxide. After the intramolecular reduction and protonation of the superoxide,

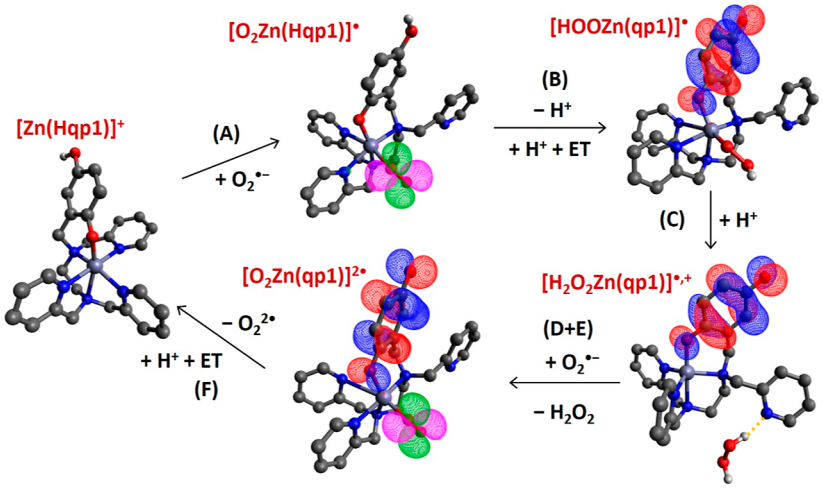

Figure 2. Molecular orbitals hosting the unpaired electrons of all species pertaining to the proposed dominant $[Zn(Hqp1)]^+/[Zn(qp1)]$ (**mer**) cycle. The reaction steps are listed in parentheses. The $[O_2Zn(qp1)]^{2\bullet}$ intermediate bears two unpaired electrons (open-shell singlet) and the related orbitals are depicted with different colors (blue/red vs green/purple). ET signifies electron transfer from either the ligand to the $O_2^{\bullet-}$ (step B) or the reverse direction (step F).

https://doi.org/10.1021/acs.jpca.3c07403
J. Phys. Chem. A 2024, 128, 1491−1500

the resultant HOO^- is further protonated by the phosphate buffer; as long as the **mer** conformation is maintained, reaction step C is exergonic by 9.6 kcal/mol (Table 1). This is followed by the exergonic release of the H_2O_2 ligand ($\Delta G = -5.7$ kcal/mol) in step D. The free energies of the intermediates for [Zn(qp1)] continue to be lower than those for [Zn(Hqp1)], indicating that the semiquinone anion continues to stabilize the intermediates.

Reaction Steps E and F—Coordination of the Second Equiv of Superoxide and Its Oxidation to Dioxygen. The coordination of the second equivalent of $O_2^{\bullet-}$ to $[Zn(qp1)]^{\bullet,+}$ resembles the other superoxide-binding event seen in step A in that it is endergonic for all **mer**, **fac**/**cis**, and **fac**/**trans** cases by 8−14 kcal/mol (Table 1 and Figure 1). The two unpaired electrons on $O_2^{\bullet-}$ and $qp_1^{\bullet-}$ can couple into an open-shell singlet or a triplet. The triplet density is always lower by 0.6−0.7 kcal/mol for all three species.

The coordination of $O_2^{\bullet-}$ to $[Zn(Hqp1)]^{\bullet 2+}$ was less straightforward. We were not able to find a stable $O_2^{\bullet-}$ + $[Zn(Hqp1)]^{\bullet 2+}$ coordination complex. Instead, when we started from the geometry of the stable $O_2^{\bullet-}$ + $[Zn(qp1)]^{\bullet,+}$ coordination complex $[O_2Zn(qp1)]^{2\bullet}$ ($S = 1$) and added a proton to the oxygen terminus of $qp1^{2-}$ to form $[O_2Zn(Hqp1)]^{2\bullet,+}$, we obtained a weakly bound complex of an O_2 molecule and $[Zn(Hqp1)]^+$. An analogous reaction occurs with $O_2^{\bullet-}$ + $[Zn(qp1)]^{2+}$, which creates a weakly bound complex of O_2 and $[Zn(qp1)]^{\bullet+}$. These observations agree with the electronic state of the semiquinone ligand in the three cases. The $qp1^{\bullet-}$ ligand of $[Zn(qp1)]^{\bullet,+}$ is less willing to accept an electron compared to qp1 and $Hqp1^{\bullet}$ of $[Zn(qp1)]^{2+}$ and $[Zn(Hqp1)]^{\bullet 2+}$, respectively (see above; reaction step B). Consequently, we believe that the oxidation of the $O_2^{\bullet-}$ occurs in an intramolecular fashion for $[Zn(qp1)]^{\bullet,+}$ but with rapid outer-sphere mechanisms for $[Zn(qp1)]^{2+}$ and $[Zn(Hqp1)]^{\bullet 2+}$.

The resulting $O_2^{2\bullet}$ ($S = 1$)−$[Zn(Hqp1)]^+$ molecular complex is lower in energy than $[O_2Zn(qp1)]^{2\bullet}$, and the black and red FEDs of Figure 1 cross at this point. Therefore, in solution, $[O_2Zn(qp1)]^{2\bullet}$ will get protonated and spontaneously eject a molecule of O_2. The $[Zn(Hqp1)]^+$ byproduct can relax back to its optimal structure, closing the catalytic cycle.

Overall, the acid/base chemistry of the quinol-derived portion of the H_2qp1 ligand plays important roles in the catalysis. The initial deprotonation of the nonmetal-bound hydroxyl group greatly facilitates the transfer of an electron from the quinolate to $O_2^{\bullet-}$, and its subsequent reprotonation is needed to complete the catalytic cycle. The highest-energy species intermediate on the proposed path, the product of step C with [Zn(qp1)], is 12.7 kcal/mol higher in energy than the initial reactants $[Zn(Hqp1)]^+$ (Figure 1, Table 1).

The molecular orbitals hosting one unpaired electron for the intermediates corresponding to the proposed lowest-energy path $[Zn(Hqp1)]^+$/[Zn(qp1)] (**mer**) route (black/red lines of Figure 1) are shown in Figure 2. The first $O_2^{\bullet-}$ initially keeps its electron in the π_{OO}^* orbital until the attachment of the first proton induces the migration of one electron from one delocalized π orbital of the quinolate (leaving it singly occupied) to O_2H. This step is facilitated by the deprotonation of the quinol. Upon reduction, the latter moiety becomes a basic HOO^- that can accept a second proton to yield H_2O_2. During the last step, the electron of the second $O_2^{\bullet-}$ (green/purple orbital) couples into a triplet with the electron localized on the semiquinolate anion (red/blue orbital). One of the two electrons of the doubly occupied π^* orbital of $O_2^{\bullet-}$ migrates to the same orbital of the quinol-derived portion of the ligand, yielding $O_2^{2\bullet}$ ($S = 1$) and a quinolate dianion. This last step is facilitated by protonation of the quinolate dianion.

The Mulliken charges and spin densities for all oxygen atoms are shown in Figure S3 of the SI and are in complete agreement with the molecular orbitals' picture. The charges of the oxygen atoms in the quinol remain practically unchanged throughout the process. For the structures with an unpaired electron in the quinol ring, half of the spin density belongs to the carbon atoms, with the two oxygen atoms sharing the other half of the electron in a ∼3:1 ratio. The distal oxygen has a higher spin density than the metal-bound oxygen. The charge and spin density on the O_2 moiety are about −0.6 and 1.0 when it is formally $O_2^{\bullet-}$, and the charge ranges from −0.85 to −0.89 when it is formally an OOH^- or HOOH.

The Zn(II) serves three roles. As mentioned previously, the first role of the metal ion is to stabilize $qp1^{2-}$. The second role is to coulombically attract and coordinate $O_2^{\bullet-}$. Manganese-containing SOD mimetics with higher positive charges tend to catalyze superoxide dismutation more efficiently.[16,25,26,29,31,58] The ability of Zn(II) to place superoxide in close proximity to $qp1^{2-}$ enables facile electron transfer from $qp1^{2-}$ to $O_2^{\bullet-}$. The third role is to hinder the coordination of other competitively binding anions, particularly phosphate. Phosphate inhibition has been found to decrease the activities of manganese-containing SOD mimics, as assessed by the k_{cat} values of the reactions between the compounds and superoxide,[17,41,55] but not those of zinc-quinol catalysts.[37,38] The ΔG for superoxide coordination remains practically the same when Mn(II) is substituted for Zn(II): 3.7 and 3.7 kcal/mol, respectively. With Mn(III), the more positive charge renders the free energy for superoxide coordination negative ($\Delta G = -0.5$ kcal/mol). However, Mn(III) also has a higher affinity for PO_4^{3-}. The ΔG values for the formation of the Zn(II)/PO_4^{3-}, Mn(II)/PO_4^{3-}, and Mn(III)/PO_4^{3-} species are −7.8, −7.1, and −11.8 kcal/mol, respectively. The phosphate inhibition observed for manganese-containing SOD mimics is correlated with the ability of manganese to access the +3 oxidation state. The inability of Zn(II) to be oxidized to a more positive metal ion discourages phosphate coordination, preventing phosphate from competitively inhibiting the coordination and activation of superoxide.

Formation and Possible Catalytic Roles of the *para*-Quinone Species. The quinol can potentially be doubly deprotonated and oxidized by two electrons to form a *para*-quinone group; the loss of two net H atoms yields the qp1 form of the ligand. The key intermediate for this reactivity is $[Zn(qp1)]^{\bullet,+}$, which is produced at reaction step D of the proposed mechanism; this is the lowest-energy intermediate of the FED for [Zn(qp1)] (**mer**) (Figure 1). When $O_2^{\bullet-}$ binds to $[Zn(qp1)]^{\bullet,+}$, there are two possible routes. First, an electron can be transferred from the superoxide to the ligand with the aid of a proton attached to the ligand, producing O_2 and leaving the catalyst in the most stable $[Zn(Hqp1)]^+$ form. The second path occurs via an electron transfer to the opposite direction to create the *para*-quinone species $[Zn(qp1)]^{2+}$, with the addition of two protons converting O_2^{2-} into H_2O_2. The first path is exergonic by 6.4 kcal/mol [−9.5−(−3.1); Table 1], and the second path is endergonic by 2.7 kcal/mol [102.0−99.3; Table 1]. $[Zn(qp1)]^{2+}$ can also form from the disproportionation of $[Zn(qp1)]^{\bullet+}$; two of these ions can

https://doi.org/10.1021/acs.jpca.3c07403
J. Phys. Chem. A 2024, 128, 1491−1500

react to form [Zn(qp1)] and $[Zn(qp1)]^{2+}$. The disproportionation is unfavorable as well with ΔG = 21.3 kcal/mol.

Consequently, we believe that the H_2O_2 and O_2 production rely predominantly on the $qp1^{\bullet-}$/$Hqp1^{-}$ redox couple and that the doubly oxidized qp1 form of the ligand is rarely accessed. Nonetheless, the energies of the intermediates corresponding to the qp1/$qp1^{\bullet-}$ redox couple are not entirely prohibitive, accounting for the $[Zn(qp1)]^{2+}$ species that have been experimentally observed during and after catalysis.[37]

Preparation and Analysis of a Phenolic Version of $[Zn(H_2qp1)]^{2+}$: $[Zn(Hpp1)]^{2+}$. Even though the quinolic portion of the ligand does not need to donate two electrons for catalysis to proceed, the ability of the distal, noncoordinating hydroxyl group to deprotonate, yielding a dianionic ligand, is essential to the superoxide dismutation. To experimentally confirm this, we prepared a Zn(II) complex with Hpp1, $[Zn(Hpp1)](OTf)_2$ (**3**); the ligand is identical to H_2qp1 except for the lack of the second hydroxyl group (Scheme 2).[40] The phenol from Hpp1 should be able to coordinate to Zn(II) analogously to quinol from H_2qp1. The synthesis proceeds smoothly, and the identity and purity of the complex were confirmed by mass spectrometry and elemental analysis. Attempts to crystallize and structurally characterize **3** have thus far been unsuccessful. The NMR spectra are inconsistent with the existence of a single conformer in solution. This was anticipated since similarly complicated solution-state behavior was observed for the Zn(II)−H_2qp1 complex.[37]

Phenol and quinol have nearly identical pK_a values in water (9.9), but the second hydroxyl group does render quinol more susceptible to oxidation, as indicated by its lower O−H bond dissociation energy: 81.5 vs 89.9 kcal mol^{-1}, as assessed by measurements in DMSO.[59] Deprotonating the second hydroxyl group further weakens the remaining O−H bond to 73.0 kcal mol^{-1}. The phenol-for-quinol substitution would therefore be anticipated to hinder step B in our proposed mechanism (Figure 1, Table 1).

We analyzed the ability of **3** to serve as a SOD mimic using stopped-flow kinetics measurements on the direct reactions between **3** and $O_2^{\bullet-}$ in 60 mM MOPS buffered to pH 7.4 (Figure 3). This medium was found to support SOD mimicry for both **1** and **2**.[37,38] Unlike **1** and **2**, **3** does not accelerate the decomposition of $O_2^{\bullet-}$ in a buffered aqueous solution, even at a relatively high concentration of 4.5 μM. The removal of the second hydroxyl group completely eliminates catalysis by precluding the Hpp1 species from accessing the lower-energy intermediates available to H_2qp1.

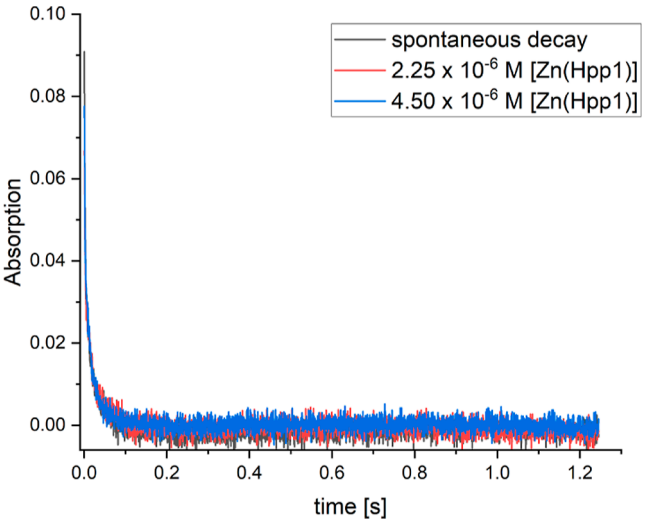

Figure 3. Kinetic traces of superoxide decomposition at 250 nm by **3** in 60 mM MOPS buffer, pH 7.4, and ionic strength of 150 mM. Either 0 (black), 2.25 (red), or 4.45 μM (blue) of **3** is present. The Zn(II) has no noticeable impact on the degradation of superoxide.

CONCLUSIONS

Our calculations support the previously proposed inner-sphere dismutation of superoxide by Zn(II) complexes with quinol-containing ligands. The activity relies upon superoxide being able to bind *cis* to the quinol-derived portion of the ligand. Keeping the quinol-derived portion of the ligand *mer* with the two amines appears to lower the free energies of the intermediates in the catalytic cycle. A constraining ligand that enforces such a conformation may further reduce the barrier for zinc-catalyzed superoxide dismutation.

The ability to deprotonate the nonmetal-bound OH group in the quinol-derived portion of the ligand lowers the energies of key intermediates. Specifically, the deprotonation of the OH group in $[O_2Zn(Hqp1)]^{\bullet}$ enables the transfer of one electron from the quinol-derived unit to the coordinated superoxide, which transiently becomes O_2^{2-} before it abstracts a proton from the solution. Substituting a phenol for the quinol removes the second hydroxyl group and is predicted to disrupt the catalysis of superoxide dismutation; we confirmed this experimentally. The second proton transfer to HOO^{-} is generally easier and can be improved if proper ligand design can place it across from the Zn−O bond of the quinol-derived portion of the ligand. The reduction of the semiquinone anion is facilitated by its initial protonation. Finally, Zn(II) benefits the reactivity by stabilizing $qp1^{2-}$. The inability of this metal to access the +3 oxidation state discourages phosphate coordination, thereby preventing this competing anion from inhibiting the reactivity.

ASSOCIATED CONTENT

Supporting Information

The Supporting Information is available free of charge at https://pubs.acs.org/doi/10.1021/acs.jpca.3c07403.

Reaction steps and orbital contours for intermediates of superoxide dismutation catalyzed by [Zn(qp1)] (**fac**/**cis** and **fac**/**trans**) and $[Zn(qp1)]^{\bullet+}$ (**mer**) and MN15/6-31g(d,p) Cartesian coordinates and energies for all discussed intermediates (PDF)

AUTHOR INFORMATION

Corresponding Authors

Evangelos Miliordos − *Department of Chemistry and Biochemistry, Auburn University, Auburn, Alabama 36849, United States;* orcid.org/0000-0003-3471-7133; Email: emiliord@auburn.edu

Christian R. Goldsmith − *Department of Chemistry and Biochemistry, Auburn University, Auburn, Alabama 36849, United States;* orcid.org/0000-0001-7293-1267; Email: crgoldsmith@auburn.edu

Authors

Jamonica L. Moore − *Department of Chemistry and Biochemistry, Auburn University, Auburn, Alabama 36849, United States*

Segun V. Obisesan − *Department of Chemistry and Biochemistry, Auburn University, Auburn, Alabama 36849, United States*

Julian Oppelt − *Department of Chemistry, Ludwig-Maximilians-Universität München, 81377 München, Germany*

Ivana Ivanović-Burmazović − *Department of Chemistry, Ludwig-Maximilians-Universität München, 81377 München, Germany*

Complete contact information is available at: https://pubs.acs.org/10.1021/acs.jpca.3c07403

Notes

The authors declare no competing financial interest.

■ ACKNOWLEDGMENTS

We thank Auburn University (AU) and the National Science Foundation (NSF-CHE-1662875 and NSF-CHE-1954336) for financial support. E.M. is grateful for the financial support from the James E. Land endowment (AU). We also thank Dr. Ralph Puchta for early advice on functional and basis set optimizations.

■ REFERENCES

(1) Abreu, I. A.; Cabelli, D. E. Superoxide Dismutases- A Review of the Metal-Associated Mechanistic Variations. *Biochim. Biophys. Acta* **2010**, *1804*, 263−274.

(2) Sheng, Y.; Abreu, I. A.; Cabelli, D. E.; Maroney, M. J.; Miller, A.-F.; Teixeira, M.; Valentine, J. S. Superoxide Dismutases and Superoxide Reductases. *Chem. Rev.* **2014**, *114* (7), 3854−3918.

(3) Mosley, R. L.; Benner, E. J.; Kadiu, I.; Thomas, M.; Boska, M. D.; Hasan, K.; Laurie, C.; Gendelman, H. E. Neuroinflammation, Oxidative Stress, and the Pathogenesis of Parkinson's Disease. *Clin. Neurosci. Res.* **2006**, *6* (5), 261−281.

(4) Fearon, I. M.; Faux, S. P. Oxidative Stress and Cardiovascular Disease: Novel Tools Give (Free) Radical Insight. *J. Mol. Cell. Cardiol.* **2009**, *47* (3), 372−381.

(5) Roberts, C. K.; Sindhu, K. K. Oxidative Stress and Metabolic Syndrome. *Life Sci.* **2009**, *84* (21−22), 705−712.

(6) Eskici, G.; Axelsen, P. H. Copper and Oxidative Stress in the Pathogenesis of Alzheimer's Disease. *Biochemistry* **2012**, *51* (32), 6289−6311.

(7) AbdulSalam, S. F.; Thowfeik, F. S.; Merino, E. J. Excessive Reactive Oxygen Species and Exotic DNA Lesions as an Exploitable Liability. *Biochemistry* **2016**, *55* (38), 5341−5352.

(8) Ahmed, M. I.; Gladden, J. D.; Litovsky, S. H.; Lloyd, S. G.; Gupta, H.; Inusah, S.; Denney, T., Jr.; Powell, P.; McGiffin, D. C.; Dell'Italia, L. J. Increased Oxidative Stress and Cardiomyocyte Myofibrillar Degeneration in Patients with Chronic Isolated Mitral Regurgitation and Ejection Fraction > 60%. *J. Am. Coll. Cardiol.* **2010**, *55* (7), 671−679.

(9) Kinnula, V. L. Production and Degradation of Oxygen Metabolites During Inflammatory States in the Human Lung. *Curr. Drug Targets: Inflammation Allergy* **2005**, *4* (4), 465−470.

(10) Abouhashem, A. S.; Singh, K.; Azzazy, H. M. E.; Sen, C. K. Is Low Alveolar Type II Cell SOD3 in the Lungs of Elderly Linked to the Observed Severity of COVID-19? *Antioxid. Redox Signaling* **2020**, *33* (2), 59−65.

(11) Laforge, M.; Elbim, C.; Frère, C.; Hémadi, M.; Massaad, C.; Nuss, P.; Benoliel, J.-J.; Becker, C. Tissue Damage from Neutrophil-Induced Oxidative Stress in COVID-19. *Nat. Rev. Immunol.* **2020**, *20* (9), 515−516.

(12) Riley, D. P.; Weiss, R. H. Manganese Macrocyclic Ligand Complexes as Mimics of Superoxide Dismutase. *J. Am. Chem. Soc.* **1994**, *116* (1), 387−388.

(13) Riley, D. P.; Schall, O. F. Structure-Activity Studies and the Design of Synthetic Superoxide Dismutase (SOD) Mimetics as Therapeutics. *Adv. Inorg. Chem.* **2006**, *59*, 233−263.

(14) Riley, D. P.; Lennon, P. J.; Neumann, W. L.; Weiss, R. H. Toward the Rational Design of Superoxide Dismutase Mimics: Mechanistic Studies for the Elucidation of Substituent Effects on the Catalytic Activity of Macrocyclic Manganese(II) Complexes. *J. Am. Chem. Soc.* **1997**, *119* (28), 6522−6528.

(15) Riley, D. P. Functional Mimics of Superoxide Dismutase Enzymes as Therapeutic Agents. *Chem. Rev.* **1999**, *99* (9), 2573−2588.

(16) Senft, L.; Moore, J. L.; Franke, A.; Fisher, K. R.; Scheitler, A.; Zahl, A.; Puchta, R.; Fehn, D.; Ison, S.; Sader, S.; Ivanović-Burmazović, I.; Goldsmith, C. R. Quinol-Containing Ligands Enable High Superoxide Dismutase Activity by Modulating Coordination Number, Charge, Oxidation States and Stability of Manganese Complexes throughout Redox Cycling. *Chem. Sci.* **2021**, *12* (31), 10483−10500.

(17) Kenkel, I.; Franke, A.; Dürr, M.; Zahl, A.; Dücker-Benfer, C.; Langer, J.; Filipović, M. R.; Yu, M.; Puchta, R.; Fiedler, S. R.; Shores, M. P.; Goldsmith, C. R.; Ivanović-Burmazović, I. Switching between Inner- and Outer-Sphere PCET Mechanisms of Small-Molecule Activation: Superoxide Dismutation and Oxygen/Superoxide Reduction Reactivity Deriving from the Same Manganese Complex. *J. Am. Chem. Soc.* **2017**, *139* (4), 1472−1484.

(18) Ching, H. Y. V.; Kenkel, I.; Delsuc, N.; Mathieu, E.; Ivanović-Burmazović, I.; Policar, C. Bioinspired Superoxide-Dismutase Mimics: The Effects of Functionalization with Cationic Polyarginine Peptides. *J. Inorg. Biochem.* **2016**, *160*, 172−179.

(19) Mathieu, E.; Bernard, A.-S.; Delsuc, N.; Quévrain, E.; Gazzah, G.; Lai, B.; Chain, F.; Langella, P.; Bachelet, M.; Masliah, J.; Seksik, P.; Policar, C. A Cell-Penetrant Manganese Superoxide Dismutase (MnSOD) Mimic Is Able To Complement MnSOD and Exerts an Antiinflammatory Effect on Cellular and Animal Models of Inflammatory Bowel Diseases. *Inorg. Chem.* **2017**, *56* (5), 2545−2555.

(20) Vincent, A.; Thauvin, M.; Quévrain, E.; Mathieu, E.; Layani, S.; Seksik, P.; Batinic-Haberle, I.; Vriz, S.; Policar, C.; Delsuc, N. Evaluation of the Compounds Commonly Known as Superoxide Dismutase and Catalase Mimics in Cellular Models. *J. Inorg. Biochem.* **2021**, *219*, 111431.

(21) Mathieu, E.; Bernard, A.-S.; Quévrain, E.; Zoumpoulaki, M.; Iriart, S.; Lung-Soong, C.; Lai, B.; Medjoubi, K.; Henry, L.; Nagarajan, S.; Poyer, F.; Scheitler, A.; Ivanović-Burmazović, I.; Marco, S.; Somogyi, A.; Seksik, P.; Delsuc, N.; Policar, C. Intracellular Location Matters: Rationalization of the Anti-Inflammatory Activity of a Manganese(II) Superoxide Dismutase Mimic Complex. *Chem. Commun.* **2020**, *56* (57), 7885−7888.

(22) Policar, C. Mimicking SOD, Why and How: Bio-Inspired Manganese Complexes as SOD Mimic. In *Redox-Active Therapeutics. Oxidative Stress in Applied Basic Research and Clinical Practice.*; Batinić-Haberle, I., Rebouças, J., Spasojević, I., Eds.; Springer: Cham, 2016.

(23) Batinić-Haberle, I.; Rebouças, J. S.; Spasojević, I. Superoxide Dismutase Mimics: Chemistry, Pharmacology, and Therapeutic Potential. *Antioxid. Redox Signaling* **2010**, *13* (6), 877−918.

(24) Tovmasyan, A.; Carballal, S.; Ghazaryan, R.; Melikyan, L.; Weitner, T.; Maia, C. G. C.; Reboucas, J. S.; Radi, R.; Spasojevic, I.; Benov, L.; Batinic-Haberle, I. Rational Design of Superoxide Dismutase (SOD) Mimics: The Evaluation of the Therapeutic Potential of New Cationic Mn Porphyrins with Linear and Cyclic Substituents. *Inorg. Chem.* **2014**, *53* (21), 11467−11483.

(25) Salvemini, D.; Wang, Z.-Q.; Zweier, J. L.; Samouilov, A.; Macarthur, H.; Misko, T. P.; Currie, M. G.; Cuzzocrea, S.; Sikorski, J. A.; Riley, D. P. A Nonpeptidyl Mimic of Superoxide Dismutase with Therapeutic Activity in Rats. *Science* **1999**, *286* (5438), 304−306.

(26) Aston, K.; Rath, N.; Naik, A.; Slomczynska, U.; Schall, O. F.; Riley, D. P. Computer-Aided Design (CAD) of Mn(II) Complexes: Superoxide Dismutase Mimetics with Catalytic Activity Exceeding the Native Enzyme. *Inorg. Chem.* **2001**, *40* (8), 1779−1789.

(27) Bonetta, R. Potential Therapeutic Applications of MnSODs and SOD-Mimetics. *Chem. - Eur. J.* **2018**, *24* (20), 5032−5041.
(28) Anderson, C. M.; Allen, B. G.; Sun, W.; Lee, C. M.; Agarwala, S.; Venigalla, M.; Greenberg, L.; Adkins, D.; Chen, Y.; Zhen, W.; Mould, D.; Holmlund, J.; Brill, J.; Sonis, S.; Buatti, J. Phase 1b/2a Trial of Superoxide (SO) Dismutase (SOD) Mimetic GC4419 to Reduce Chemoradiation Therapy-Induced Oral Mucositis (OM) in Patients With Oral Cavity or Oropharyngeal Carcinoma (OCC). *Int. J. Radiat. Oncol., Biol., Phys.* **2016**, *94* (4), 869−870.
(29) Batinic-Haberle, I.; Spasojevic, I. 25 Years of Development of Mn Porphyrins — from Mimics of Superoxide Dismutase Enzymes to Thiol Signaling to Clinical Trials: The Story of Our Life in the USA. *J. Porphyrins Phthalocyanines* **2019**, *23* (11n12), 1326−1335.
(30) Batinic-Haberle, I.; Rajic, Z.; Tovmasyan, A.; Reboucas, J. S.; Ye, X.; Leong, K. W.; Dewhirst, M. W.; Vujaskovic, Z.; Benov, L.; Spasojevic, I. Diverse Functions of Cationic Mn(III) N-substituted Pyridylporphyrins, Recognized as SOD Mimics. *Free Radical Biol. Med.* **2011**, *51*, 1035−1053.
(31) Batinić-Haberle, I.; Liochev, S. I.; Spasojević, I.; Fridovich, I. A Potent Superoxide Dismutase Mimic: Manganese *β*-Octabromo-meso-tetrakis-(N-methylpyridinium-4-yl) Porphyrin. *Arch. Biochem. Biophys.* **1997**, *343* (2), 225−233.
(32) DeFreitas-Silva, G.; Rebouças, J. S.; Spasojević, I.; Benov, L.; Idemori, Y. M.; Batinić-Haberle, I. SOD-Like Activity of Mn(II) *β*-Octabromo-meso-tetrakis(N-methylpyridinium-3-yl)porphyrin Equals That of the Enzyme Itself. *Arch. Biochem. Biophys.* **2008**, *477* (1), 105−112.
(33) Zhang, D.; Busch, D. H.; Lennon, P. L.; Weiss, R. H.; Neumann, W. L.; Riley, D. P. Iron(III) Complexes as Superoxide Dismutase Mimics: Synthesis, Characterization, Crystal Structure, and Superoxide Dismutase (SOD) Activity of Iron(III) Complexes Containing Pentaaza Macrocyclic Ligands. *Inorg. Chem.* **1998**, *37* (5), 956−963.
(34) Riley, D. P.; Henke, S. L.; Lennon, P. J.; Weiss, R. H.; Neumann, W. L.; Rivers, W. J., Jr; Aston, K. W.; Sample, K. R.; Rahman, H.; Ling, C.-S.; Shieh, J.-J.; Busch, D. H.; et al. Synthesis, Characterization, and Stability of Manganese(II) C-Substituted 1,4,7,10,13-Pentaazacyclopentadecane Complexes Exhibiting Superoxide Dismutase Activity. *Inorg. Chem.* **1996**, *35* (18), 5213−5231.
(35) Goldstein, S.; Samuni, A.; Hideg, K.; Merenyi, G. Structure-Activity Relationship of Cyclic Nitroxides as SOD Mimics and Scavengers of Nitrogen Dioxide and Carbonate Radicals. *J. Phys. Chem. A* **2006**, *110* (10), 3679−3685.
(36) Ali, S. S.; Hardt, J. I.; Quick, K. L.; Sook Kim-Han, J.; Erlanger, B. F.; Huang, T.-T.; Epstein, C. J.; Dugan, L. L. A Biologically Effective Fullerene (C_{60}) Derivative with Superoxide Dismutase Mimetic Properties. *Free Radical Biol. Med.* **2004**, *37* (8), 1191−1202.
(37) Ward, M. B.; Scheitler, A.; Yu, M.; Senft, L.; Zillmann, A. S.; Gorden, J. D.; Schwartz, D. D.; Ivanović-Burmazović, I.; Goldsmith, C. R. Superoxide Dismutase Activity Enabled by a Redox-Active Ligand rather than Metal. *Nat. Chem.* **2018**, *10* (12), 1207−1212.
(38) Moore, J. L.; Oppelt, J.; Senft, L.; Franke, A.; Scheitler, A.; Dukes, M. W.; Alix, H. B.; Saunders, A. C.; Karbalaei, S.; Schwartz, D. D.; Ivanović-Burmazović, I.; Goldsmith, C. R. Diquinol Functionality Boosts the Superoxide Dismutase Mimicry of a Zn(II) Complex with a Redox-Active Ligand while Maintaining Catalyst Stability and Enhanced Activity in Phosphate Solution. *Inorg. Chem.* **2022**, *61* (49), 19983−19997.
(39) Yu, M.; Ambrose, S. L.; Whaley, Z. L.; Fan, S.; Gorden, J. D.; Beyers, R. J.; Schwartz, D. D.; Goldsmith, C. R. A Mononuclear Manganese(II) Complex Demonstrates a Strategy to Simultaneously Image and Treat Oxidative Stress. *J. Am. Chem. Soc.* **2014**, *136* (37), 12836−12839.
(40) Obisesan, S. V.; Rose, C.; Farnum, B. H.; Goldsmith, C. R. Co(II) Complex with a Covalently Attached Pendent Quinol Selectively Reduces O_2 to H_2O. *J. Am. Chem. Soc.* **2022**, *144* (50), 22826−22830.
(41) Friedel, F. C.; Lieb, D.; Ivanović-Burmazović, I. Comparative Studies on Manganese-Based SOD Mimetics, Including the Phosphate Effect, by Using Global Spectral Analysis. *J. Inorg. Biochem.* **2012**, *109*, 26−32.
(42) Bielski, B. H. J.; Cabelli, D. E.; Arudi, R. L.; Ross, A. B. Reactivity of HO_2/O_2^- Radicals in Aqueous Solution. *J. Phys. Chem. Ref. Data* **1985**, *14* (4), 1041−1100.
(43) Yu, H. S.; He, X.; Li, S. L.; Truhlar, D. G. MN15: A Kohn-Sham Global-Hybrid Exchange-Correlation Density Functional with Broad Accuracy for Multi-Reference and Single-Reference Systems and Noncovalent Interactions. *Chem. Sci.* **2016**, *7* (8), 5032−5051.
(44) Clark, T.; Chandrasekhar, J.; Spitznagel, G. W.; Schleyer, P. V. R. Efficient Diffuse Function-Augmented Basis Sets for Anion Calculations. III. The 3-21+G Basis Set for First-Row Elements, Li-F. *J. Comput. Chem.* **1983**, *4* (3), 294−301.
(45) Ditchfield, R.; Hehre, W. J.; Pople, J. A. Self-Consistent Molecular-Orbital Methods. IX. An Extended Gaussian-Type Basis for Molecular-Orbital Studies of Organic Molecules. *J. Chem. Phys.* **1971**, *54* (2), 724−728.
(46) Hariharan, P. C.; Pople, J. A. The Influence of Polarization Functions on Molecular Orbital Hydrogenation Energies. *Theor. Chim. Acta* **1973**, *28* (3), 213−222.
(47) Hehre, W. J.; Ditchfield, R.; Pople, J. A. Self—Consistent Molecular Orbital Methods. XII. Further Extensions of Gaussian—Type Basis Sets for Use in Molecular Orbital Studies of Organic Molecules. *J. Chem. Phys.* **1972**, *56* (5), 2257−2261.
(48) Rassolov, V. A.; Pople, J. A.; Ratner, M. A.; Windus, T. L. 6-31G* Basis Set for Atoms K Through Zn. *J. Chem. Phys.* **1998**, *109* (4), 1223−1229.
(49) Ervin, K. M.; Anusiewicz, I.; Skurski, P.; Simons, J.; Lineberger, W. C. The Only Stable State of O_2^- Is the $X^2\Pi_g$ Ground State and It (Still!) Has an Adiabatic Electron Detachment Energy of 0.45 eV. *J. Phys. Chem. A* **2003**, *107* (41), 8521−8529.
(50) Khan, S. N.; Miliordos, E. Methane to Methanol Conversion Facilitated by Transition-Metal Methyl and Methoxy Units: The Cases of $FeCH_3^+$ and $FeOCH_3^+$. *J. Phys. Chem. A* **2019**, *123* (26), 5590−5599.
(51) Claveau, E. E.; Heller, E. R.; Richardson, J. O.; Miliordos, E. Methane against Methanol: The Tortoise and the Hare of the Oxidation Race. *J. Phys. Chem. Lett.* **2023**, *14* (39), 8749−8754.
(52) Marenich, A. V.; Cramer, C. J.; Truhlar, D. G. Universal Solvation Model Based on Solute Electron Density and on a Continuum Model of the Solvent Defined by the Bulk Dielectric Constant and Atomic Surface Tensions. *J. Phys. Chem. B* **2009**, *113* (18), 6378−6396.
(53) Frisch, M. J.; T, G. W.; Schlegel, H. B.; Scuseria, G. E.; Robb, M. A.; Cheeseman, J. R.; Scalmani, G.; Barone, V.; Petersson, G. A.; Nakatsuji, H.; et al. *Gaussian 16*; Gaussian, Inc.: Wallingford CT, 2016.
(54) Suresh, S.; Chandra Srivastava, V.; Mani Mishra, I. Adsorption of Hydroquinone in Aqueous Solution by Granulated Activated Carbon. *J. Environ. Eng.* **2011**, *137* (12), 1145−1157.
(55) Lieb, D.; Friedel, F. C.; Yawer, M.; Zahl, A.; Khusniyarov, M. M.; Heinemann, F. W.; Ivanović-Burmazović, I. Dinuclear Seven-Coordinate Mn(II) Complexes: Effect of Manganese(II)-Hydroxo Species on Water Exchange and Superoxide Dismutase Activity. *Inorg. Chem.* **2013**, *52* (1), 222−236.
(56) Ivanović-Burmazović, I. Catalytic Dismutation vs. Reversible Binding of Superoxide. *Adv. Inorg. Chem.* **2008**, *60*, 59−100.
(57) Weekley, C. M.; Kenkel, I.; Lippert, R.; Wei, S.; Lieb, D.; Cranwell, T.; Wedding, J. L.; Zillmann, A. S.; Rohr, R.; Filipovic, M. R.; Ivanović-Burmazović, I.; Harris, H. H. Cellular Fates of Manganese(II) Pentaazamacrocyclic Superoxide Dismutase (SOD) Mimetics: Fluorescently Labeled MnSOD Mimetics, X-ray Absorption Spectroscopy, and X-ray Fluorescence Microscopy Studies. *Inorg. Chem.* **2017**, *56* (11), 6076−6093.
(58) Batinic-Haberle, I.; Tovmasyan, A.; Spasojevic, I. Mn Porphyrin-Based Redox-Active Drugs: Differential Effects as Cancer Therapeutics and Protectors of Normal Tissue Against Oxidative Injury. *Antioxid. Redox Signaling* **2018**, *29* (16), 1691−1724.

https://doi.org/10.1021/acs.jpca.3c07403
J. Phys. Chem. A 2024, 128, 1491−1500

(59) Bordwell, F. G.; Cheng, J. Substituent Effects on the Stabilities of Phenoxyl Radicals and the Acidities of Phenoxyl Radical Cations. *J. Am. Chem. Soc.* **1991**, *113* (5), 1736−1743.

https://doi.org/10.1021/acs.jpca.3c07403
J. Phys. Chem. A 2024, 128, 1491−1500